



## Research paper

## Use of aligned triphenylamine-based radicals in a porous framework for promoting photocatalysis



Yan-Xi Tan, Yan-Ping He, Daqiang Yuan\*, Jian Zhang\*

State Key Laboratory of Structural Chemistry, Fujian Institute of Research on the Structure of Matter, Chinese Academy of Sciences, Fuzhou, 350002, PR China

## ARTICLE INFO

## Keywords:

Metal-organic framework  
Triphenylamine-based radical  
Photoinduced electron transfer  
Heterogeneous catalyst  
Mannich photocatalysis

## ABSTRACT

The Ca-MOF **FIR-29** is synthesized and exhibits a honeycomb lattice of hexagonal channels with an aperture of  $\sim 16 \text{ \AA}$ , giving a BET surface area of  $2061 \text{ m}^2 \text{ g}^{-1}$ . The consecutive slipped  $\pi \cdots \pi$  stacking interactions of photoactive tris((4-carboxyl)phenylduryl)amine (TCPA) groups on the surface of hexagonal channels makes it an effective photocatalyst for catalyzing the typical Mannich photocatalysis, forming  $\beta$ -tetrahydroisoquinoline ketones in high isolated yields. Catalytic activity for **FIR-29** is about 2.7 times enhancement over that for mesoporous DUT-63 consisted of discrete TCPA groups without any intermolecular interaction. This is mainly due to the fact that the rigid compact stacking of tri([1,1'-biphenyl]-4-yl)amine (TBPA) is conducive to form stable TBPA radical, and is optimal for electron or energy transfer to expedite the reactivity of  $\text{sp}^3$  carbon atoms and allow higher photocatalytic conversion.

Dedicated to professor Xin[HYPHEN]Tao Wu on the occasion of his 80th

## 1. Introduction

In the past decades, visible-light-driven photocatalysis as an eco-friendly and energy-efficient method for organic synthesis has been extensively explored [1–6]. Compared with traditional noble metal photocatalysts, organic dyes have recently attracted much attention of synthetic chemists because their promising characteristics of efficient visible-light absorption, enhanced stability, and modification susceptibility promote their application in photocatalysis [7–14]. For example, triphenylamine (TPA) and its derivatives have excellent hole-transport properties and have been widely used to construct hole-transport materials for efficient photoredox reactions [15,16]. However, the homogeneous catalysis of these TPA-based complexes makes their recycling and products separation difficult, which will further delay their practical applications in photocatalytic processes [17]. An effective approach to resolve this issue centers is to trap these TPA-based complexes into porous solid materials, making easy catalysts reuse and products purification [18–23].

Metal-organic frameworks (MOFs) are interesting hybrid solids with ordered infinite networks consisting of organic bridging ligands and inorganic nodes [24–32]. The unique porous structure of MOFs encapsulating photoactive organic groups allows them to demonstrate considerable promise in photocatalysis [26,33–42]. Recently, to overcome the current limitation of visible-light-driven photocatalysis and

enhance photocatalytic conversion of poorly active chemical bonds in organic synthesis, a significant consecutive photoinduced electron transfer (conPET) process[43] of the perylene diimide (PDI) radical anion was applied to a Zn-PDI MOF for the reduction of aryl halides [33]. Although TPA derivatives can't perform such conPET process similar to PDI units, long-range  $\pi \cdots \pi$  stacking of TPA derivatives with conjugated systems, such as tri([1,1'-biphenyl]-4-yl)amine (TBPA), can support some favorable factors for photocatalysis, including 1) the formation of stable radical with high local concentration; 2) a strong attraction to aromatic substrate molecules; 3) their packing state being optimal for electron or energy transfer [33]. These favorable factors endow desirable photocatalysis potential of TPA derivatives. Especially, the incorporation of well-organized TBPA fragments into MOFs represents a promising approach to heterogenize these photoconversions and to overcome the restrictions of the homogeneous process. Tris((4-carboxyl)phenylduryl)amine ( $\text{H}_3\text{TCPA}$ ), a trigonal ligand that contains the photoactive TBPA group, has been employed to build some MOFs used for their gas sorption and optical properties [44–48], but none of them shows visible-light-driven photocatalysis in organic synthesis, because the TBPA units in these MOFs were not aligned appropriately.

In this paper, the redox-active Ca-MOF,  $\{[\text{Ca}_5(\text{TCPA})_3(\text{H}_2\text{O})_6]^+ \}_n \text{nNO}_3^-$ , **FIR-29**, FIR denotes Fujian Institute of Research) shows hexagonal channels with an aperture of  $16 \text{ \AA}$  and well-organized aggregation of photoactive TBPA moieties as aryl radicals, making it an effective photocatalyst. The typical oxidative Mannich reaction[49] of *N*-phenyltetrahydroisoquinoline and

\* Corresponding author.

E-mail addresses: [ydq@fjirsm.ac.cn](mailto:ydq@fjirsm.ac.cn) (D. Yuan), [zhj@fjirsm.ac.cn](mailto:zhj@fjirsm.ac.cn) (J. Zhang).

nonactivated ketones under mild conditions is selected as model substrates to examine the feasibility of the optimal photoinduced electron transfer (PET) process in the consecutive long-range  $\pi\cdots\pi$  stacking of the stable TBPA radials.

## 2. Experimental

### 2.1. Materials and methods

Commercially available reagents were used as received. Thermal gravimetric analysis data were obtained with an NETZSCH STA 449C analyzer. All samples and reference ( $\text{Al}_2\text{O}_3$ ) were enclosed in a platinum crucible and were heated from 25 to 700 °C at a rate of 10 °C/min under an  $\text{N}_2$  atmosphere. X-ray powder diffraction (XRPD) patterns were collected on a Rigaku Mini 600 X-ray diffractometer with  $\text{Cu K}\alpha$  radiation ( $\lambda = 1.5406 \text{ \AA}$ ) at a scanning rate of 5°/min for  $2\theta$  ranging from 4° to 40°. Simulated XRPD patterns were calculated using Mercury from corresponding single-crystal structural models.  $^1\text{H}$  NMR spectra were recorded on a Bruker Avance 400 (400.1 MHz for  $^1\text{H}$  NMR). The deuterated solvents used are indicated in the experimental part. EPR spectra were recorded on a Bruker BioSpin E500 EPR spectrometer with a 100 kHz magnetic field modulation at room temperature equipped with a 16 mW ultraviolet lamp. Gas adsorption measurement was performed in the ASAP 2020 System. Optical diffuse reflectance spectra were measured at room temperature on a Perkin Elmer Lambda-950 UV/Vis/NIR spectrophotometer by using  $\text{BaSO}_4$  as baseline sample.

### 2.2. Preparation of $\{[\text{Ca}_5(\text{TCPA})_3(\text{H}_2\text{O})_6]^+\}_n\text{NO}_3^-$ (FIR-29)

$\text{H}_3\text{TCPA}$  (60 mg),  $\text{Ca}(\text{NO}_3)_2 \cdot 4\text{H}_2\text{O}$  (50 mg), 4 mL dimethylacetamide (DMA) and 0.5 mL  $\text{H}_2\text{O}$  in an 8 mL vial was stirred for 30 min, and then sealed and heated in an oven at 120 °C for 3 days. The vial was then cooled to room temperature. After washing with fresh DMA, yellow triangular-prism-shaped crystals were obtained in pure form (Yield: 70 mg, 57% based on  $\text{H}_3\text{TCPA}$ ).

### 2.3. X-ray crystallography

The diffraction data of **FIR-29** was collected on a SuperNova diffractometer equipped with a copper micro-focus X-ray sources ( $\lambda = 1.5406 \text{ \AA}$ ) and an Atlas CCD detector under 100 K. Empirical absorption correction used spherical harmonics, implemented in SCALE3 ABSPACK scaling algorithm. The structure was solved by direct methods and refined with full-matrix least-squares technique using *SHELXL-2014*. All non-hydrogen atoms were refined with anisotropic displacement parameters. The diffused electron densities resulting from these residual solvent molecules were removed from the dataset using the *SQUEEZE* routine of *PLATON* and refined further using the data generated. The contents of the solvent region are not represented in the unit cell contents in the crystal data. Crystal data of **FIR-29**:  $\text{C}_{117}\text{H}_{72}\text{N}_3\text{O}_{24}\text{Ca}_5$ ,  $M_r = 2104.17$ , space group  $P3_121$ ,  $a = 37.0787(5) \text{ \AA}$ ,  $c = 30.0922(7) \text{ \AA}$ ,  $V = 35828.9(13) \text{ \AA}^3$ ,  $Z = 6$ ,  $D_c = 0.585 \text{ g cm}^{-3}$ ,  $F_{000} = 6522$ ,  $\text{CuK}\alpha$  radiation,  $\lambda = 1.54184 \text{ \AA}$ ,  $T = 100.0(2) \text{ K}$ , 48768 reflections collected, 29178 unique ( $R_{\text{int}} = 0.0757$ ). Final  $\text{Goof} = 1.095$ ,  $R1 = 0.0894$ ,  $wR2 = 0.2211$ ,  $R$  indices based on 6522 reflections with ( $I > 2\sigma(I)$ ) (refinement on  $F^2$ ).

### 2.4. Typical experimental procedure for catalysis

Representative procedure: to a 10 mL Schleck flask equipped, crystalline powder of **FIR-29** (5.0 mmol% based on  $\text{Ca}_5$  cluster), the respective substrate (0.5 mmol) and L-proline (6 mg) were added into dry MeCN (3 mL) and acetone (1 mL) via stirring. Then the reaction mixture was stirred under open air for 8 h at a distance of about 5 cm from a 7 W blue LEDs lamp. Upon the completion of reaction, as monitored by TLC (petroleum ether: ethyl acetate = 4:1), the crude

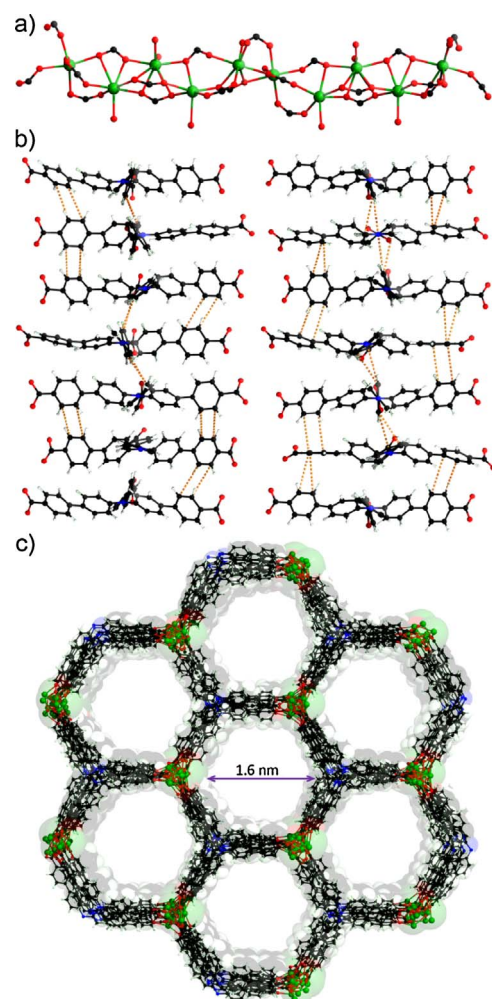


**Fig. 1.** (a) A Ca-COO chain running along the c axis; (b) Two parallel stacking arrays of TCPA fragments; (c) 3D framework showing nanoporous hexagonal channels.

reaction mixture was purified by flash chromatography on silica gel (silica: 200–300 mesh; eluent: petroleum ether/ethyl acetate (4:1) to provide the corresponding pure product.

## 3. Results and discussion

### 3.1. Crystal structure

The reaction of  $\text{H}_3\text{TCPA}$  and  $\text{Ca}(\text{NO}_3)_2 \cdot 6\text{H}_2\text{O}$  in a mixed DMA/ $\text{H}_2\text{O}$  solvent at 120 °C for 3 days afforded the yellow triangular-prism-shaped crystals of **FIR-29**. Single-crystal X-ray diffraction analysis reveals that **FIR-29** crystallizes in a chiral space group  $P3_121$ . In each asymmetric unit, the five independent  $\text{Ca}^{2+}$  ions with the 6-, 7- or 8-coordinated geometries (Fig. 1a) are bridged by carboxyl groups to form a metallic pentamer  $\text{Ca}_5(\text{COO})_9$  and are further linked by three carboxyl groups in an ABBA... arrangement, giving rise to an infinitely positive Ca-COO chain along the c axis. The TCPA ligands around the Ca-COO chain are closely arranged along the c direction, showing intermolecular interactions of consecutive long-range slipped  $\pi\cdots\pi$  stacking with the distance between two C atoms from the phenyl rings of TCPA ligands measured at 3.5–3.8 Å (Fig. 1b) [50]. The favorable factor may support optimal electron or energy transfer process and endow desirable photocatalysis potential of **FIR-29**. In the structure of **FIR-29**, each rod-like Ca-COO chain is then connected to other six chains by long trigonal bridging ligand TCPA to form a 3D rod-packing architecture (Fig. 1c). Such rod-and-spacer approach has been proved

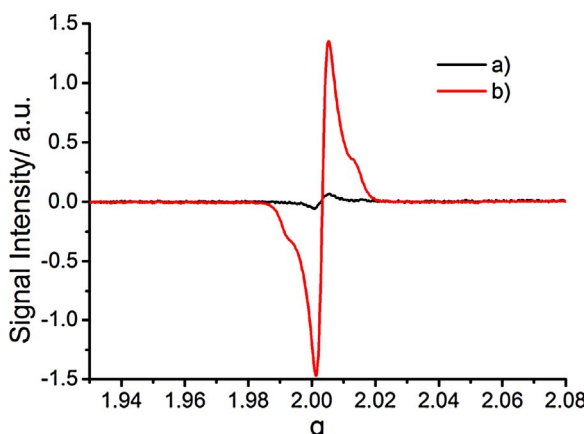


Fig. 2. EPR spectra of  $K_3$ TCPA (a), and FIR-29a(b).

to be one of the most effective methods to obtain porous metal-carboxylate structures because of the absence of interpenetration [51–53]. Furthermore, this open framework of **FIR-29** exhibits a honeycomb lattice of hexagonal channels along the *c* axis, and the aperture for each hexagonal channel is approximately 16 Å (including van der Waals radii). The solvent-accessible volume (including charge-balancing anions) of **FIR-29** is about 67.1% of the total crystal volume estimated by the *PLATON* program [54]. The free spaces are occupied by the disordered solvent molecules and charge-balancing anions.

### 3.2. TGA, EPR and UV/Vis spectrum

The phase purity of **FIR-29** is testified by powder X-ray diffraction (PXRD) (Fig. S2b). The Thermogravimetric analysis (TGA) curve of **FIR-29** reveals a weight loss of 40.1% under 200 °C, corresponding to the release of guest molecules (Fig. S1). **FIR-29** was soaked in MeCN solution for 3 days and then activated under high vacuum at 150 °C for 8 h, forming the hollow phase **FIR-29a**. The electron paramagnetic resonance (EPR) spectrum (Fig. 2) of **FIR-29a** (28.9 mg, 0.04 mmol TCPA) shows a peak at  $g = 2.003$ , indicating that the nitrogen atoms of the organic TBPA species incorporated in the host solid of **FIR-29a** have been oxidized to free radicals and show much higher signal intensity after irradiation of blue LEDs for 60 min, which is about 19 times enhancement over that for  $K_3$ TCPA (28.8 mg, 0.04 mmol TCPA) under the same conditions. Slipped  $\pi$  stacking interactions between TCPA ligands supports their excellent ability to delocalize and migrate excitons, which in turn supports the formation of stable TBPA radical anions in the host compound. The UV/Vis spectrum of **FIR-29** shows a strong absorption band at 416 nm, maybe corresponding to the  $n-\pi^*$  and  $\pi-\pi^*$  transition of TCPA ligands (Fig. S3). The band gap energy of **FIR-29** determined from Kubelka–Munk function is 2.58 eV.

### 3.3. Gas sorption

To examine the permanent porosity of **FIR-29**, the gas sorption of the desolvated form (**FIR-29a**) was studied. The  $N_2$  sorption isotherms at 77 K reveal an  $N_2$  uptake of  $681 \text{ cm}^3 \text{ g}^{-1}$  at 1 bar, giving a BET surface area of  $2061 \text{ m}^2 \text{ g}^{-1}$  and a micropore volume of  $1.05 \text{ cm}^3 \text{ g}^{-1}$  (Fig. 3). A pore size distribution analysis by non-localized density functional theory (NLDFT) methods utilizing  $N_2$  gas at 77 K shows a broad distribution of 1.0–1.8 nm (Fig. S4). Clearly, the pore size of 1.6 nm takes advantage of numbers in **FIR-29a**. Such excellent sorption property is due to the  $\pi-\pi$  interaction between TCPA ligands, which is beneficial to stabilize the honeycomb channels in **FIR-29**.

### 3.4. Mannich reaction of *N*-phenyltetrahydroisoquinolines with acetone

Tris(4-bromophenyl)aminium hexachloroantimonate, as a well-

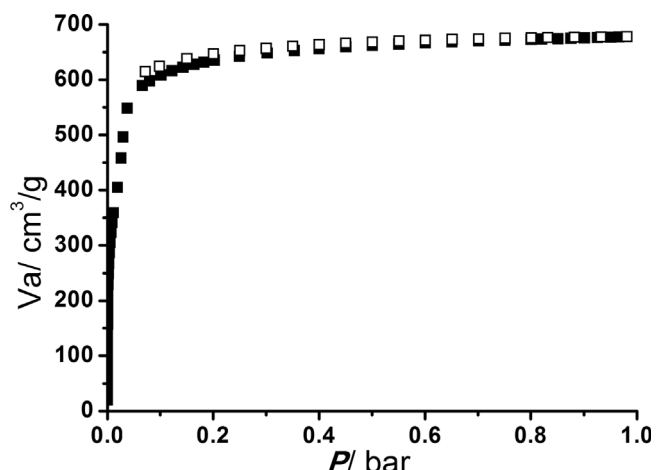


Fig. 3. Gas sorption isotherms of  $N_2$  at 77 K for **FIR-29a**.

known stable radical cation salt, was demonstrated to be an efficient initiator for the oxidative Mannich reaction of tertiary amines and nonactivated ketones under mild neutral conditions [55]. The organized aggregation of TBPA groups in **FIR-29** creates stable free radicals and also leaves considerable space for the ingress and egress of fitted substrates and products, leading to its potential application of photocatalysis in an oxidative Mannich reaction catalyzed by free radicals. By using MOF **FIR-29** as visible light photocatalysts under mild reaction conditions, we became interested in investigating the PET process of aligned TBPA radicals by using the typical Mannich-type reaction of *N*-phenyltetrahydroisoquinoline (A) with acetone (B), and L-proline (to form the enamine nucleophile) as a probe reaction, which involves the activation of  $sp^3$  carbon atoms and the formation of C–C bonds [56]. 5 mmol% (based on  $Ca_5$  cluster) photocatalyst **FIR-29** was used as a heterogeneous photocatalyst for the above aerobic Mannich-type reaction of under irradiation of blue LEDs at ambient conditions for 8 h. As can be seen in Entries 1–3 of Table 1, the controlling experiments show that each component, including light, oxygen and the MOF photocatalyst, is necessary for the reaction. Once these conditions were met, formation of the desired cross-coupling product (C) in good yield was observed (Entry 8). The  $\beta$ -tetrahydroisoquinolone ketone (C), the principal product was confirmed by  $^1\text{H}$  NMR spectroscopy (See Supplementary Information). For photocatalyst **FIR-29**, the isolated yield of the reaction is 85% after 8 h, which is much higher than that (46%) of  $K_3$ TCPA (Entry 4). An explanation for this behavior may be that the rigid compact stacking of TBPA is conducive to optimal electron or energy transfer pathway during the PET process of the TBPA radical expediting the functionalization of the  $sp^3$  C–H bond adjacent to a nitrogen atom in A and allowing higher photocatalytic conversion. Additionally, the extended conjugated system in **FIR-29** endows on TBPA exceptional optical stability in combination with strong visible-light absorption, both conditions which are favourable for the application of this heterogeneous process [33]. In order to deeply understand significance of such PET process in the long-range  $\pi-\pi$  stacking of the stable TBPA radicals for the Mannich reaction, a mesoporous MOF (DUT-63) [57], in which the Cu paddle-wheel units are linked by discrete TCPA ligands without any intermolecular interaction (Such as, H-bond and  $\pi-\pi$  interactions) (Fig. S5 and S6), is also employed to perform the same Mannich reaction. As expected, the isolated yield of 32% (Entry 5) is very low and even lower than that of  $K_3$ TCPA, because the energy conferred by discrete TBPA radials may be inefficient to convert the  $sp^3$  C–H bond. [33]. Some MOFs have achieved considerable success in this field, however costly and toxic metal reagents often act as catalysts. For example, Sn-mediated MOF (UNLPF-12) and UiO-68-Se achieved a yield of 98% and 94% for the aerobic Mannich reaction of *N*-phenyl-1,2,3,4-tetrahydroisoquinoline with acetone under air [56,58].  $Au^{3+}$

**Table 1**

The visible light induced Mannich reactions of *N*-phenyl-1,2,3,4-tetrahydroisoquinoline (A) with acetone (B).

Entry	Conditions	Substituent	Yield/% <sup>a</sup>
1 <sup>b</sup>	no catalyst	-R = -H	trace
2 <sup>c</sup>	no light	-R = -H	trace
3 <sup>d</sup>	no oxygen	-R = -H	trace
4 <sup>e</sup>	K <sub>3</sub> TCPA	-R = -H	46
5 <sup>f</sup>	DUT-63	-R = -H	32
6 <sup>g</sup>	Eosin B	-R = -H	42
7 <sup>h</sup>	Eosin Y	-R = -H	40
8 <sup>i</sup>	FIR-29	-R = -H	85
9 <sup>j</sup>	FIR-29	-R = -H	36
10 <sup>k</sup>	FIR-29	-R = -H	36
11 <sup>l</sup>	FIR-29	-R = -H	83
12 <sup>m</sup>	FIR-29	-R = -H	82
13	FIR-29	-R = -Br	88
14	FIR-29	-R = -Me	81
15	FIR-29	-R = -OMe	89

<sup>a</sup> Yield of the isolated products.

<sup>b</sup> The reaction without any catalyst.

<sup>c</sup> The reaction in the presence of FIR-29 was stirred under the dark and air atmosphere.

<sup>d</sup> The reaction mixture was strictly degassed and then irradiated under an Ar atmosphere.

<sup>e</sup> 15 mmol% K<sub>3</sub>TCPA.

<sup>f</sup> 15 mmol% (based on TCPA<sup>3</sup> ligand) DUT-63.

<sup>g</sup> 15 mmol% Eosin B used as a photocatalyst.

<sup>h</sup> 15 mmol% Eosin Y used as a photocatalyst.

<sup>i</sup> Run 1.

<sup>j</sup> Yield after 3 h.

<sup>k</sup> The filtration test by removing the catalyst FIR-29 after 3 h and continuing the reaction for another 5 h.

<sup>l</sup> Run 2.

<sup>m</sup> Run 3.

complexes-loading MOF achieved an isolated yield of 84.2% under a solvent-saturated oxygen atmosphere [59]. More importantly, the catalytic activity of FIR-29 is much higher than two simple dyes, Eosin B and Eosin Y, as homogeneous catalysts (Entries 6–7), and bears comparison with the reported PDMS-RB sponge photocatalyst by anchoring Rose Bengal dye [60]. As a green photocatalyst without costly and toxic metal, FIR-29 shows comparable catalytic activity to aforementioned MOFs and promotes photocatalysis via the optimal PET process of well-organized ligands rather than metal reagents.

The heterogeneity of photocatalyst FIR-29 was confirmed by removal of the catalyst after 3 h (yield: 36%), which resulted in essentially no further production of the final product C, showing that the heterogeneous photocatalyst FIR-29 fails to attract any catalytically active species into the reaction system (Entries 9–10). The reusability of the photocatalyst FIR-29 was also investigated by using the same batch of FIR-29 for three successive catalytic cycles of this reaction. The results indicate that catalytic activity of FIR-29 remains fairly consistent after three cycles (yields:  $\geq 82\%$ ) (Entries 11–12). XRPD measurements of the recycled photocatalyst revealed maintenance of its crystalline structure, confirming the stability of FIR-29 in the catalytic system (Fig. S2c). We further extended the scope of this aerobic Mannich reaction catalyzed by the photocatalyst FIR-29 (Table 1) and observed that A with various substituent groups could be coupled with acetone readily to afford the desired products in good to excellent yields (Entries 13–15). It's worth noting that *N*-phenyl-tetrahydroisoquinoline derivatives with electron-donating and electron-withdrawing groups on the phenyl rings are all compatible in the aerobic C–C coupling reaction.

Previous research indicated  $O_2^{-\cdot}$  was the active intermediate

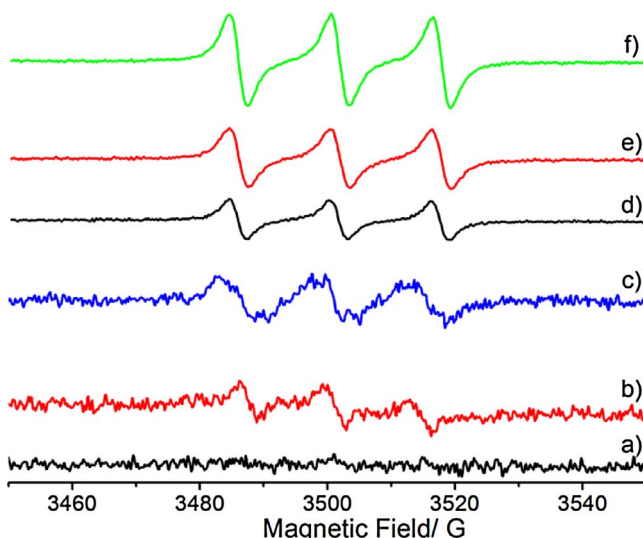
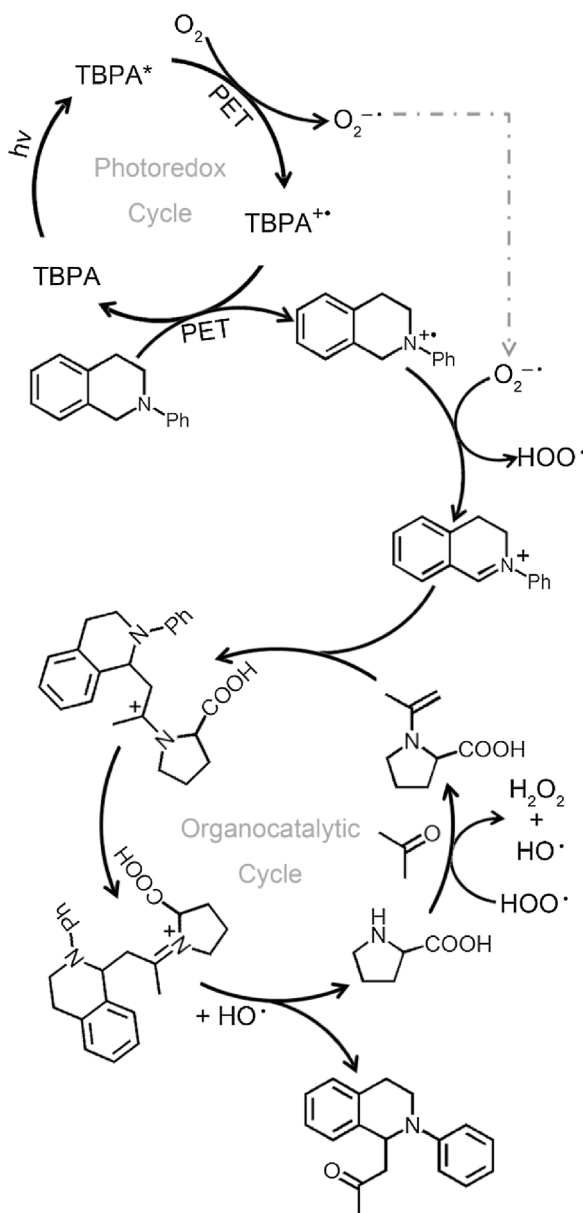


**Fig. 4.** EPR spectra of the  $CH_3CN$  solution with DMPO (a); FIR-29 and DMPO (b); FIR-29, A, and DMPO (c) under irradiation of blue LEDs for 60 min. EPR spectra of the  $CH_3CN$  solution with TEMP (a); FIR-29 and TEMP (b); FIR-29, A and TEMP (c) under irradiation of blue LEDs for 20 min. (For interpretation of the references to colour in this figure legend, the reader is referred to the web version of this article.)

species in the visible-light-driven aerobic CDC reaction [8,58,61–63]. To understand the photocatalytic process of FIR-29 in detail, the EPR measurements are conducted in 5,5-dimethyl-1-pyrroline-N-oxide (DMPO) and 2,2,6,6-tetramethylpiperidine (TEMP), which are used to capture superoxide radical anion  $O_2^{-\cdot}$  and singlet oxygen  $^1O_2$ , respectively. As shown in Fig. 4, upon irradiation of the  $CH_3CN$  mixture of FIR-29 and DMPO in the air, the formation of  $O_2^{-\cdot}$  under the reaction conditions is confirmed by EPR spectroscopy (Fig. 4c). As shown in Fig. 4d–4e, no  $^1O_2$  can be generated during the photocatalysis process. These findings indicate that  $O_2^{-\cdot}$  is the active intermediate species in the reaction. Mechanistically, we proposed that the highly reactive iminium intermediate was formed by the oxidation of the C–H bond adjacent to the nitrogen of A (Scheme 1). The TBPA array in FIR-29 accepts a number of photons from the visible light source to form the excited state TBPA\* array and then is immediately quenched by oxygen via a PET process, generating the array of radical TBPA<sup>+</sup> cations and the superoxide radical anion  $O_2^{-\cdot}$ . The array of radical TBPA<sup>+</sup> cation accepts electrons from molecule A forming the radical anion A<sup>+</sup> and simultaneously reducing TBPA<sup>+</sup> to its ground state. These superoxide radical anions  $O_2^{-\cdot}$  generated by the photoredox cycle of TBPA may abstract a hydrogen atom from the radical cation A<sup>+</sup> to form the desired iminium ion A<sup>+</sup>, which enters the organocatalytic cycle and reacts with the enamine nucleophile generated by L-proline-activated acetone to give the desired product [56].

#### 4. Conclusions

In summary, we have first constructed a noble-metal-free Ca-MOF (FIR-29) with organized aggregation of photoactive TBPA groups as aryl radicals. The robust FIR-29 acts as an efficient and heterogeneous photocatalyst for aerobic Mannich reactions to form  $\beta$ -tetrahydroisoquinoline ketone products under visible light. This reaction depends upon the heterogeneity of photocatalytic transformation, and the synergistic effect of nanopores and a PET process between well-organized TBPA radicals. It is envisioned that combining organic molecular catalysts in MOFs can be an effective approach to optimizing the activity of heterogeneous catalysts for efficient photocatalysis.



**Scheme 1.** Proposed mechanism of Mannich photocatalysis for FIR-29.

## Acknowledgements

This work was financially supported by the Strategic Priority Research Program of CAS (XDB20000000), the Key Research Program of Frontier Sciences, CAS (QYZDB-SSW-SLH019), the National Nature Science Foundation of China (21390392, 21371169, 21403235, and 21603229), and the Nature Science Foundation of Fujian Province (2016J01080).

## Appendix A. Supplementary data

Supplementary data associated with this article can be found, in the online version, at <http://dx.doi.org/10.1016/j.apcatb.2017.09.054>.

## References

- J. Meeuwissen, J.N. Reek, Supramolecular catalysis beyond enzyme mimics, *Nature Chem.* 2 (2010) 615–621.
- D. Ravelli, D. Dondi, M. Fagnoni, A. Albini, Photocatalysis: A multi-faceted concept for green chemistry, *Chem. Soc. Rev.* 38 (2009) 1999–2011.
- A. Albini, M. Fagnoni, *Handbook of Synthetic Photochemistry*, Wiley-VCH Verlag GmbH & Co. KGaA, 2010.
- L. Zeng, X. Guo, C. He, C. Duan, Metal–organic frameworks versatile materials for heterogeneous photocatalysis, *ACS Catal.* 6 (2016) 7935–7947.
- J.C. Chu, T. Rovis, Amide-directed photoredox-catalysed C–C bond formation at unactivated  $sp^3$  C–H bonds, *Nature* 539 (2016) 272–275.
- Q. Yang, L. Zhang, C. Ye, S. Luo, L.-Z. Wu, C.-H. Tung, Visible-light-promoted asymmetric cross-dehydrogenative coupling of tertiary amines to ketones by synergistic multiple catalysis, *Angew. Chem. Int. Ed.* 56 (2017) 3694–3698.
- S. Hanessian, S. Giroux, B.L. Merner, *Design and Strategy in Organic Synthesis: From the Chiron Approach to Catalysis*, Wiley-VCH Verlag GmbH & Co. KGaA, 2013.
- X.-Z. Wang, Q.-Y. Meng, J.-J. Zhong, X.-W. Gao, T. Lei, L.-M. Zhao, Z.-J. Li, B. Chen, C.-H. Tung, L.-Z. Wu, The singlet excited state of BODIPY promoted aerobic cross-dehydrogenative-coupling reactions under visible light, *Chem. Commun.* 51 (2015) 11256–11259.
- D. Ravelli, M. Fagnoni, A. Albini, Photoorganocatalysis what for? *Chem. Soc. Rev.* 42 (2013) 97–113.
- Y.-Q. Zou, J.-R. Chen, W.-J. Xiao, Homogeneous visible-light photoredox catalysis, *Angew. Chem. Int. Ed.* 52 (2013) 11701–11703.
- C.K. Prier, D.A. Rankic, D.W. MacMillan, Visible light photoredox catalysis with transition metal complexes: applications in organic synthesis, *Chem. Rev.* 113 (2013) 5322–5363.
- L. Shi, W. Xia, Photoredox functionalization of C–H bonds adjacent to a nitrogen atom, *Chem. Soc. Rev.* 41 (2012) 7687–7697.
- J.M. Narayanan, C.R. Stephenson, Visible light photoredox catalysis: applications in organic synthesis, *Chem. Soc. Rev.* 40 (2011) 102–113.
- T.P. Yoon, M.A. Ischay, J. Du, Visible light photocatalysis as a greener approach to photochemical synthesis, *Nature Chem.* 2 (2010) 527–532.
- J.R. Pinzon, D.C. Gasca, S.G. Sankaranarayanan, G. Bottari, T. Torres, D.M. Guidi, L. Echegoyen, Photoinduced charge transfer and electrochemical properties of triphenylamine  $I_h$ -Sc $_{3}$ N@C $_{60}$  donor-acceptor conjugates, *J. Am. Chem. Soc.* 131 (2009) 7727–7734.
- H. Zhao, W.-Z. Yuan, L. Tang, J.-Z. Sun, H. Xu, A. Qin, Y. Mao, J.-K. Jin, B.-Z. Tang, Hybrids of triphenylamine-functionalized polyacetylenes and multiwalled carbon nanotubes: high solubility, strong donor-acceptor interaction, and excellent photoconductivity, *Macromolecules* 41 (2008) 8566–8574.
- X. Wang, W. Lu, Z.-Y. Gu, Z. Wei, H.-C. Zhou, Topology-guided design of an anionic bor-network for photocatalytic [Ru(bpy) $_{3}$ ] $^{2+}$  encapsulation, *Chem. Commun.* 52 (2016) 1926–1929.
- T. Araya, M. Jia, J. Yang, P. Zhao, K. Cai, W. Ma, Y. Huang, Resin modified MIL-53(Fe) MOF for improvement of photocatalytic performance, *Appl. Catal. B* 203 (2017) 768–777.
- Y. Gao, S. Li, Y. Li, L. Yao, H. Zhang, Accelerated photocatalytic degradation of organic pollutant over metal–organic framework MIL-53(Fe) under visible LED light mediated by persulfate, *Appl. Catal. B* 202 (2017) 165–174.
- Y.-P. Yuan, L.-S. Yin, S.-W. Cao, G.-S. Xu, C.-H. Li, C. Xue, Improving photocatalytic hydrogen production of metal–organic framework UiO-66 octahedrons by dye-sensitization, *Appl. Catal. B* 168 (2015) 572–576.
- J. Liu, H. Shi, Q. Shen, C. Guo, G. Zhao, Efficiently photoelectrocatalyze CO $_{2}$  to methanol using Ru(II)-pyridyl complex covalently bonded on TiO $_{2}$  nanotube arrays, *Appl. Catal. B* 210 (2017) 368–378.
- J.-L. Wang, C. Wang, K. E. deKraft, W. Lin, cross-linked polymers with exceptionally high Ru(bpy) $_{3}$  $^{2+}$  loadings for efficient heterogeneous photocatalysis, *ACS Catal.* 2 (2012) 417–424.
- P. Wu, C. He, J. Wang, X. Peng, X. Li, Y. An, C. Duan, Photoactive chiral metal–organic frameworks for light-driven asymmetric  $\alpha$ -alkylation of aldehydes, *J. Am. Chem. Soc.* 134 (2012) 14991–14999.
- G. Cai, H.-L. Jiang, A modulator-induced defect-formation strategy to hierarchically porous metal–organic frameworks with high stability, *Angew. Chem. Int. Ed.* 56 (2017) 563–567.
- B.S. Gelfand, R.P. Huynh, R.K. Mah, G.K. Shimizu, Mediating order and modulating porosity by controlled hydrolysis in a phosphonate monoester metal–organic framework, *Angew. Chem. Int. Ed.* 55 (2016) 14614–14617.
- A. Dhakshinamoorthy, A.M. Asiri, H. Garcia, Metal–organic frameworks catalyzed C–C and C–heteroatom coupling reactions, *Chem. Soc. Rev.* 44 (2015) 1922–1947.
- T. Zhang, W. Lin, Metal–organic frameworks for artificial photosynthesis and photocatalysis, *Chem. Soc. Rev.* 43 (2014) 5982–5993.
- H. Wu, F. Yang, X.-L. Lv, B. Wang, Y. Zhang, M. Zhao, J.-R. Li, A stable porphyrinic metal–organic framework: pore-functionalization by high-density carboxylic groups for proton conduction, *J. Mater. Chem. A* 5 (2017) 14525–14529.
- J. Zhao, Q. Wang, C. Sun, T. Zheng, L. Yan, M. Li, K. Shao, X. Wang, Z. Su, A hexanuclear cobalt metal–organic framework for efficient CO $_{2}$  reduction under visible light, *J. Mater. Chem. A* 5 (2017) 12498–12505.
- S. Rapti, D. Sarma, S. Diamantis, E. Skliri, G.S. Armatas, A. Tsipis, Y.S. Hassan, M.H. Alkordi, C.D. Malliakas, M. Kanatzidis, T. Lazarides, J.C. Plakatouras, E. Manos, All in one porous material: exceptional sorption and selective sensing of hexavalent chromium by a Zr $^{4+}$  MOF, *J. Mater. Chem. A* 5 (2017) 14707–14719.
- A. Aziz, A.R. Ruiz-Salvador, N.C. Hernandez, S. Calero, S. Hamad, R. Grau-Crespo, Porphyrin-based metal–organic frameworks for solar fuel synthesis photocatalysis: band gap tuning via iron substitutions, *J. Mater. Chem. A* 5 (2017) 11894–11904.
- S. Yuan, T.-F. Liu, D. Feng, J. Tian, K. Wang, J. Qin, Q. Zhang, Y.-P. Chen, M. Bosch, L. Zou, S.J. Teat, S.J. Dalgarno, H.-C. Zhou, A single crystalline porphyrinic titanium metal–organic framework, *Chem. Sci.* 6 (2015) 3926–3930.
- L. Zeng, T. Liu, C. He, D. Shi, F. Zhang, C. Duan, Organized aggregation makes insoluble perylene diimide efficient for the reduction of aryl halides via consecutive visible light-induced electron-transfer processes, *J. Am. Chem. Soc.* 138 (2016)

3958–3961.

[34] X. Yu, L. Wang, S.M. Cohen, Photocatalytic metal-organic frameworks for organic transformations, *CrystEngComm* 19 (2017) 4126–4136.

[35] A. Crake, K.C. Christoforidis, A. Kafizas, S. Zafeiratos, C. Petit, CO<sub>2</sub> capture and photocatalytic reduction using bifunctional TiO<sub>2</sub>/MOF nanocomposites under UV-vis irradiation, *Appl. Catal. B* 210 (2017) 131–140.

[36] X. Liu, R. Dang, W. Dong, X. Huang, J. Tang, H. Gao, G. Wang, A sandwich-like heterostructure of TiO<sub>2</sub> nanosheets with MIL-100(Fe): A platform for efficient visible-light-driven photocatalysis, *Appl. Catal. B* 209 (2017) 506–513.

[37] D. Sun, L. Ye, Z. Li, Visible-light-assisted aerobic photocatalytic oxidation of amines to imines over NH<sub>2</sub>-MIL-125(Ti), *Appl. Catal. B* 164 (2015) 428–432.

[38] R. Liang, L. Shen, F. Jing, W. Wu, N. Qin, R. Lin, L. Wu, NH<sub>2</sub>-mediated indium metal-organic framework as a novel visible-light-driven photocatalyst for reduction of the aqueous Cr(VI), *Appl. Catal. B* 162 (2015) 245–251.

[39] J.-L. Wang, C. Wang, W. Lin, Metal-organic frameworks for light harvesting and photocatalysis, *ACS Catal.* 2 (2012) 2630–2640.

[40] J. He, J. Wang, Y. Chen, J. Zhang, D. Duan, Y. Wang, Z. Yan, A dye-sensitized Pt@UiO-66(Zr) metal-organic framework for visible-light photocatalytic hydrogen production, *Chem. Commun.* 50 (2014) 7063–7066.

[41] S. Wang, X. Wang, Multifunctional metal-organic frameworks for photocatalysis, *Small* 11 (2015) 3097–3112.

[42] A. Fateeva, P.A. Chater, C.P. Ireland, A.A. Tahir, Y.Z. Khimyak, P.V. Wiper, J.R. Darwent, M.J. Rosseinsky, A water-stable porphyrin-based metal-organic framework active for visible-light photocatalysis, *Angew. Chem. Int. Ed.* 51 (2012) 7440–7444.

[43] I. Ghosh, T. Ghosh, J.I. Bardagi, B. Konig, Reduction of aryl halides by consecutive visible light-induced electron transfer processes, *Science* 346 (2014) 725–728.

[44] Y.-P. He, Y.-X. Tan, F. Wang, J. Zhang, Microporous zinc tris[(4-carboxyl)phenylduryl]amine framework with an unusual topological net for gas storage and separation, *Inorg. Chem.* 51 (2012) 1995–1997.

[45] Y.-P. He, Y.-X. Tan, J. Zhang, Tuning a layer to a pillared-layer metal-organic framework for adsorption and separation of light hydrocarbons, *Chem. Commun.* 49 (2013) 11323–11325.

[46] Y.-P. He, Y.-X. Tan, J. Zhang, Gas sorption, second-order nonlinear optics, and luminescence properties of a multifunctional srs-type metal-organic framework built by tris(4-carboxylphenylduryl)amine, *Inorg. Chem.* 54 (2015) 6653–6656.

[47] Y.-P. He, Y.-X. Tan, J. Zhang, Guest inducing fluorescence switching in lanthanide-tris[(4-carboxyl)phenylduryl]amine frameworks integrating porosity and flexibility, *J. Mater. Chem. C* 2 (2014) 4436.

[48] H.J. Park, D.W. Lim, W.-S. Yang, T.R. Oh, M.P. Suh, A highly porous metal-organic framework: structural transformations of a guest-free MOF depending on activation method and temperature, *Chem. Eur. J.* 17 (2011) 7251–7260.

[49] W. Liu, Q. Su, P. Ju, B. Guo, H. Zhou, G. Li, Q. Wu, A hydrazone-Based covalent organic framework as an efficient and reusable photocatalyst for the cross-dehydrogenative coupling reaction of N-aryltetrahydroisoquinolines, *ChemSusChem* 10 (2017) 664–669.

[50] C. Janiak, A critical account on  $\pi$ - $\pi$  stacking in metal complexes with aromatic nitrogen-containing ligands, *J. Chem. Soc. Dalton Trans.* (2000) 3885–3896.

[51] Y.-X. Tan, Y.-P. He, Y. Zhang, Y.-J. Zheng, J. Zhang, Solvent controlled assembly of four Mn(II)-2,5-thiophenedicarboxylate frameworks with rod-packing architectures and magnetic properties, *CrystEngComm* 15 (2013) 6009–6014.

[52] Y.-X. Tan, F. Wang, Y. Kang, J. Zhang, Dynamic microporous indium(III)-4,4-oxybis(benzoate) framework with high selectivity for the adsorption of CO<sub>2</sub> over N<sub>2</sub>, *Chem. Commun.* 47 (2011) 770–772.

[53] N.L. Rosi, J. Kim, M. Eddaoudi, B. Chen, M. O'Keeffe, O.M. Yaghi, Rod packings and metal-organic frameworks constructed from rod-shaped secondary building units, *J. Am. Chem. Soc.* 127 (2005) 1504–1518.

[54] A.L. Spek, Single-crystal structure validation with the program PLATON, *J. Appl. Crystallogr.* 36 (2003) 7–13.

[55] C. Huo, M. Wu, X. Jia, H. Xie, Y. Yuan, J. Tang, Aerobic oxidative Mannich reaction promoted by catalytic amounts of stable radical cation salt, *J. Org. Chem.* 79 (2014) 9860–9864.

[56] J.A. Johnson, J. Luo, X. Zhang, Y.-S. Chen, M.D. Morton, E. Echeverría, F.E. Torres, J. Zhang, Porphyrin-metalation-mediated tuning of photoredox catalytic properties in metal-organic frameworks, *ACS Catal.* 5 (2015) 5283–5291.

[57] P. Müller, R. Grunker, V. Bon, M. Pfeffermann, I. Senkovska, M.S. Weiss, X. Feng, S. Kaskel, Topological control of 3,4-connected frameworks based on the Cu<sub>2</sub>-paddle-wheel node: tbc or pto, and why?, *CrystEngComm* 18 (2016) 8164–8171.

[58] W.-Q. Zhang, Q.-Y. Li, Q. Zhang, Y. Lu, H. Lu, W. Wang, X. Zhao, X.-J. Wang, Robust metal-organic-framework containing benzoselenadiazole for highly efficient aerobic cross-dehydrogenative coupling reactions under visible light, *Inorg. Chem.* 55 (2016) 1005–1007.

[59] C.-Y. Sun, W.-P. To, X.-L. Wang, K.-T. Chan, Z.-M. Su, C.-M. Che, Metal-organic framework composites with luminescent gold(III) complexes. Strongly emissive and long-lived excited states in open air and photo-catalysis, *Chem. Sci.* 6 (2015) 7105–7111.

[60] X. Li, Y. Li, Y. Huang, T. Zhang, Y. Liu, B. Yang, C. He, X. Zhou, J. Zhang, Organic sponge photocatalysis, *Green Chem.* 19 (2017) 2925–2930.

[61] C.-J. Wu, J.-J. Zhong, Q.-Y. Meng, T. Lei, X.-W. Gao, C.-H. Tung, L.-Z. Wu, Cobalt-catalyzed cross-dehydrogenative coupling reaction in water by visible light, *Org. Lett.* 17 (2015) 884–887.

[62] A.G. Condie, J.C. González-Gómez, C.R.J. Stephenson, Visible-light photoredox catalysis: aza-Henry reactions via C–H functionalization, *J. Am. Chem. Soc.* 132 (2010) 1464–1465.

[63] Q.-Y. Meng, J.-J. Zhong, Q. Liu, X.-W. Gao, H.-H. Zhang, T. Lei, Z.-J. Li, K. Feng, B. Chen, C.-H. Tung, L.-Z. Wu, A cascade cross-coupling hydrogen evolution reaction by visible light catalysis, *J. Am. Chem. Soc.* 135 (2013) 19052–19055.